Bulk Synthesis of Graphene-Like Materials Possessing Turbostratic Graphite and Graphene Nanodomains via Combustion of Magnesium in Carbon Dioxide

Tak H. Kim[a,b], Christopher R. Merritt[a], Caterina Ducati[c], Andrew D. Bond[c], Nick Bampos[c], Christopher L. Brown*[a,b]

[a]School of Environment and Natural Science, Griffith University, 170 Kessels Road, Nathan, QLD 4112, Australia

[b]The Environmental Futures Research Institute, Griffith University, 170 Kessels Road, Nathan, QLD 4112, Australia

[c]Department of Chemistry, University of Cambridge, Lensfield Road, Cambridge CB2 1EW, United Kingdom

* Corresponding author. Fax: + 61 7 3735 7509, Email: c.l.brown@griffith.edu.au

Abstract

This study reports a gram scale synthesis of a turbostratically aligned carbon material containing regions of graphite and few-layer graphene located in carbon-only nanodomains. The material, obtained from the combustion of magnesium in a carbon dioxide atmosphere, displays 2D and layered 3D molecular architectures. Of particular interest is that the introduction of an in-air high-temperature calcination process yields a carbon material possessing discrete turbostratic structural regions, as evidenced by Raman spectroscopy, transmission electron microscopy, electron energy loss spectroscopy and X-ray powder diffraction characterisations.

1. Introduction

Although graphene is ideally a single 2D layer, ‘few-layer’ graphene of up to five sheets retains many of the interesting properties of its single-layer parent. Accordingly, a range of graphene-like materials (GLMs) possessing both 2D and layered 3D molecular architectures are under active investigation for a wide range of applications[1] such as electronics[2,3], composites[4], energy[5] and also biological[6] applications. The diversity of application drives the development of facile routes for the assembly of these materials. Thus far, a number of different approaches, such as mechanical and liquid exfoliation[7], chemical manipulation of graphite (oxidation and subsequent reduction reactions)[8], chemical vapour deposition (CVD)[9], arc discharge[2], hydrothermal[8] and microwave methods[10] have been reported. The varying methods outlined differ in the morphology, quality and quantity of graphene and carbon materials they produce. Variations within the materials include (but are not limited to) different sheet sizes, variable layer thicknesses, defect location, size and frequency, variable domain composition as well as the actual amount of usable material produced. Accordingly, much work is being undertaken to produce graphene and GLMs possessing both consistent and useful chemical and physical properties[7–10].

Differences in stacking order in carbon materials have been reported using both Raman spectroscopy (specifically by analyses of the *2D* band[11,12]), and using X-ray powder diffraction (XRD) analysis[13,14]. In Raman, phonon decoupling of a single-layer graphene (SLG) within the turbostratic graphite results in the disappearance of the multiple- component *2D* band which arises due to the random orientation of the SLGs, initiating the appearance of a single-component *2D* band[15–17]. In XRD, a turbostratic stacking of SLGs can also be differentiated since the regular *AB* pattern usually seen in multilayer graphene and graphite is replaced by a random orientation, resulting in an increased interplanar spacing, with values greater than 0.34 Å compared to ~0.33 Å for graphite[14,18].

Due to the stacking order, turbostratic carbon materials often possess altered physical properties relative to crystalline graphite[18]. It has been reported that the electronic properties for turbostratic carbon materials can be described more accurately as a quasi-monolayer graphene material[13,19], potentially making them attractive for a range of practical applications. The recent discovery of new electronic ground states in twisted graphene layers further broaden the possibilities as tuneable carbon materials[20,21].

The successful development of graphene-based applications depends on a large-scale availability of the material. Thus far, these misaligned carbon materials were demonstrated using CVD methods[14,17], which may limit the scalability. Herein, we report a large, up-scalable and reproducible synthesis of misaligned graphene-like material (GLM) using a carbon dioxide reduction method[22]. The material obtained from this synthetic route was originally reported as multilayer graphene as characterised by Raman and X-ray diffraction (XRD)[22]. Further processing and analysis of the resulting material suggests that the GLM sample prepared contains turbostratic nanodomains. The transmission electron microscopy (TEM) reveals that the GLM sample contains two dissimilar nanodomains, whilst Raman characterisation indicates that the *2D* peak in this material was comparable to the *2D* Raman peak observed in 'true' monolayer graphene, suggesting random orientations of graphene-like sheets[15–17]. Furthermore, XRD analysis further indicates that the interplanar spacing was larger than the spacing of graphite[14,18].

2. Experimental

2.1 Materials and methods

As illustrated in Scheme 1, a 5 kg block of dry ice (12 cm × 15 cm × 20 cm, local supplier) was sawn in half using a commercial band saw. A small hollow was excavated into the

centre of one half of the block which was partly filled by magnesium (Mg) ribbon (5g, Sigma Aldrich). To aid ignition, a small amount of Mg powder (0.5g, Sigma Aldrich) was placed on top of the ribbon. The Mg powder was initially ignited using a party sparkler followed by covering with the other half of the dry ice block. The magnesium ribbons were allowed to combust completely (Scheme 1, **I**). After combustion a grey-black product consisting of a mixture of magnesium oxide (MgO) and carbon material was collected. This process was repeated until the dry ice had almost fully sublimed (approximately 20 runs) after which the combined product was mechanically ground to a fine powder in a mortar and pestle. Caution must be taken since the combustion process involves a highly exothermic reaction producing heat and light.

The resulting ground material (200 g) was transferred to a 5 L beaker and 2.5 L of hydrochloric acid (3 M, Chem-Supply, Australia) was introduced and stirred overnight (16 h) to digest the MgO by-product (Scheme 1, **II**). The resulting carbon slurry was filtered and rinsed copiously with pure water until reaching pH 7. Finally, the carbon solids were collected using vacuum filtration with a 0.22 μm nylon membrane (Scheme 1, **III**). The collected sample was dried in a vacuum oven overnight at 80°C (producing **A**cid-washed **G**raphene-**L**ike **M**aterial, A-GLM). Approximately 30 g of the A-GLM was obtained after the digestions and washes.

A-GLM (30g) was divided evenly into four 30 mL porcelain crucibles and calcined in air for 4 hours in a furnace at 570 °C (20 °C·min^{-1}). Approximately 15 g of calcinated A-GLM was obtained. The calcinated A-GLM was digested again under the same digestion procedures for preparing A-GLM. Finally, the sample was filtered and dried using the same protocol (producing **P**rocessed **G**raphene-**L**ike **M**aterial, P-GLM, Scheme 1, **IV**) yielding approximately 1g.

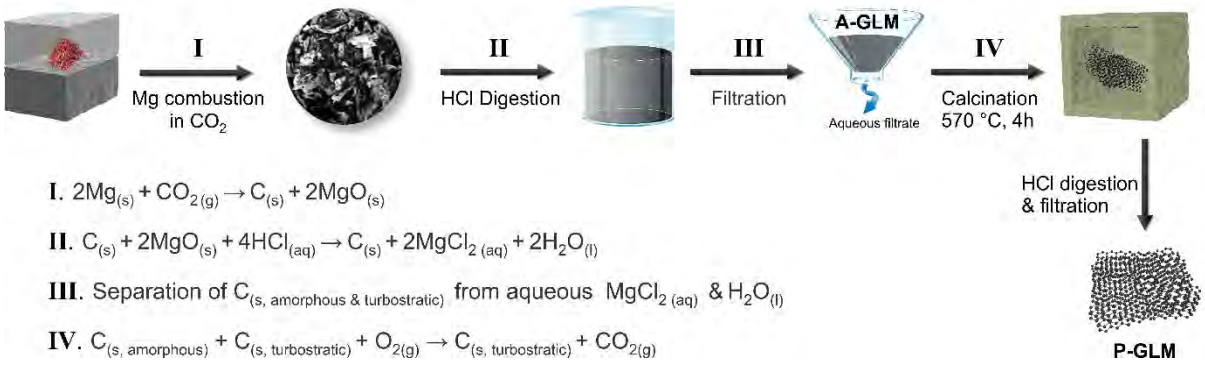

Scheme 1. Synthesis routes and their reactions for GLMs.

2.2 Instrumental

Scanning Electron Microscopic (SEM) characterisations were carried out in a JEOL JSM-7001F and the images were acquired at 15 kV accelerating voltage. Transmission Electron Microscopy (TEM) and Electron Energy Loss Spectroscopy (EELS) were performed in a FEI Tecnai Osiris 80-200 operated at 80 kV. Raman spectra were recorded on a Renishaw inVia Raman microscope equipped with a 50mV 514 nm laser. Deconvolution of the Raman spectra were performed using OriginPro software package (v9.0). X-ray Diffraction (XRD) patterns were obtained on a Panalytical X'Pert Pro instrument, using non-monochromated CuKα radiation (λ_{ave} = 1.5418 Å). A background correction was applied using the X'pert HighScore software package (v1.0b). X-ray Photoelectron Spectroscopy (XPS) spectra were acquired using a Kratos Axis ULTRA X-ray photoelectron spectrometer incorporating a 165 mm hemispherical electron energy analyser and mono Al Kα (1486.6 eV) X-ray source. Calculations of atomic concentrations and peak fittings of the high-resolution data were carried out using the CasaXPS software package (v2.2.73). Thermogravimetric Analysis (TGA) was performed in a Netzsch STA 449F3. The sample was heated to 900 °C at 5 °C·min^{-1} heating rate using either argon or air as the purge gas. Fourier transform infrared (FTIR) spectra were recorded on a Perkin Elmer Spectrum Two IR spectrometer equipped

with a diamond attenuated total reflectance (ATR) attachment and a baseline correction was applied using the PerkinElmer Spectrum software package (v10.03.09.0139).

3. Results and discussion

As described in the experimental, the synthesis involved the ignition of magnesium turnings inside a small hollow within a block of dry ice. Once ignited a dry ice lid was placed over the top of the block producing large amount of heat and light (Fig. 1 (a))[22].

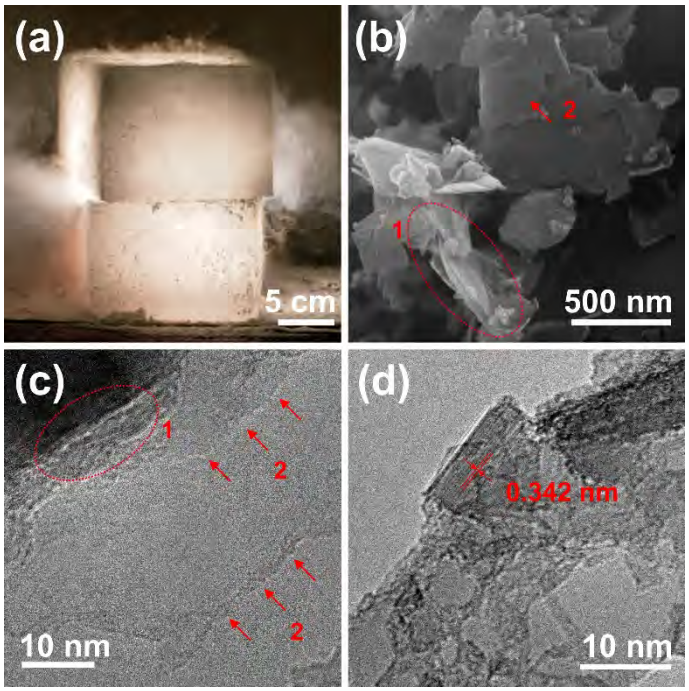

Fig. 1 - (a) Picture taken during the synthesis of GLMs, (b) Scanning Electron Microscopy (SEM), (c) Transmission Electron Microscopy (TEM) of P-GLM sample presenting (1) turbostratic nanodomains and (2) multilayer Graphene like nanodomains and (d) interlayer spacing of the turbostratic nanodomains.

Analysis of P-GLM by a scanning electron microscopy (SEM, Fig.1 (b)) revealed large, few-layer carbon sheets in which the length of larger sheets was up to 3 μm with an average length of ~1 μm. The transmission electron microscopy (TEM) in Fig.1 (c) further revealed very thin areas typical of few-layer stacked graphene sheets. Interlayer spacing of the P-GLMs were measured by XRD at ~3.42 Å (0.342 nm, Fig.1 (d)) against a value of 3.35 Å for crystalline graphite[18].

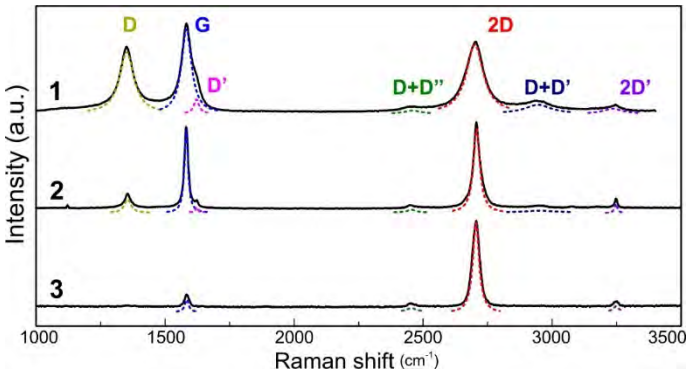

Fig. 2 - Raman spectra (514 nm) of (1) A-GLM, (2) P-GLM sample in contrast with (3) a single layer CVD graphene reference sample.

Raman spectroscopy is usually the first method for the initial characterisation of the materials arising from the various synthetic approaches to graphene and GLM syntheses. The literature is replete with information on the interpretation of Raman data, both from a practical and theoretical perspective Raman analysis affords information on both atomic structure, electronic properties and other information such as defect density and defect special distribution, all from the one experiment[11]. The typical graphene spectrum consists of several bands; the *D* and *G* bands appear around 1350 and 1580 cm^{-1} respectively, whilst the characteristic *2D* band appears at around 2700 cm^{-1}. Although the *G* and *2D* bands are always present in graphene and related polyaromatic materials[23,24], the *D* band is

associated with defects and its presence and intensity varies with the sample. Other peaks may also be present depending on the quality and defect density of the material. In single-layer graphene, the *2D* peak is a single Lorentzian peak. Addition of more layers from few-layer graphene, to multilayer graphene to graphite results in a *2D* peak that broadens and splits as the number of layers increases.

The Raman spectrum of our A-GLMs (measured at 514 nm, 2.51 eV, Fig. 2) was comparable to the spectrum reported previously[22,25] with a *D, G* and *2D* bands at 1350, 1580 and 2700 cm^{-1} respectively, indicating A-GLMs consist of few-layer graphene materials (I_{2D}/I_D = 1.37, *2D* FWHM = 79 cm^{-1}). The band positions from the Raman spectrum of the P-GLMs showed no notable changes compared to the A-GLMs and the I_{2D}/I_G ratios also showed no significant changes (I_{2D}/I_G P-GLMs = 1.78 *cf.* I_{2D}/I_G A-GLMs = 1.37). Interestingly, however, the *2D* peak from the P-GLMs was comparable to the *2D* peak from a single-layer graphene reference sample (P-GLMs *2D* FWHM = 30.5 cm^{-1} *cf.* SLG *2D* FWHM = 30.0 cm^{-1}). Although the electron microscopic results of the P-GLMs showed strong evidence of multi-layer structures, the *2D* Raman band behaves like a single- layer graphene which is comparable to the single Lorentzian *2D* band from the CVD graphene. This is due to the turbostratic (or misaligned) stacking of single graphene layers resulting in the phonon decoupling of a single-layer graphene in the P-GLM leads to the single Lorentzian peak, typical of SLG[15–17].

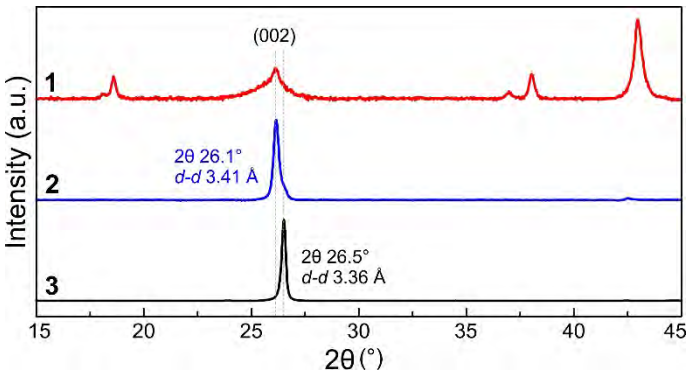

Fig. 3 - X-ray diffraction (XRD) patterns of (1) A-GLM, (2) P-GLM in contrast with (3) a graphite reference sample. In A-GLM, the prominent peaks other than 002 are attributable to MgO (periclase) and $Mg(OH)_2$ (brucite) by-products.

X-ray diffraction patterns are presented in Fig. 3. Both A-GLM and P-GLM display a prominent 002 peak at 26.1°, indicating the presence of multilayer structure[26,27]. For A-GLM, the other visible peaks ($2\theta \approx 18.6$, 37.0, 38.0 and 43.0°) can be attributed to MgO (periclase) and $Mg(OH)_2$ (brucite) by-products (see Supplementary Information for further details). The 002 peak position is identical in the P-GLM and A-GLM, indicating similar structure. The *d*-spacing of the P-GLM was measured at 3.41 Å, which is in agreement with the value obtained from the TEM characterisation (3.42 Å). Furthermore, the *d*-spacing of the graphene layers in the P-GLM is notably different from the measured graphite reference sample (P-GLMs = 3.41 Å *cf.* graphite = 3.36 Å). The greater interplanar spacing from the P-GLM, compared to the graphite, indicates the turbostratic stacking of SLGs within the P-GLM due to the randomly rotated layers and the angular disorder of the single graphene layers [14,18,28]. Some asymmetry is evident for the 002 peak of P-GLM, extending towards the *d*-spacing observed for graphite, indicative of some ordered graphite-like regions.

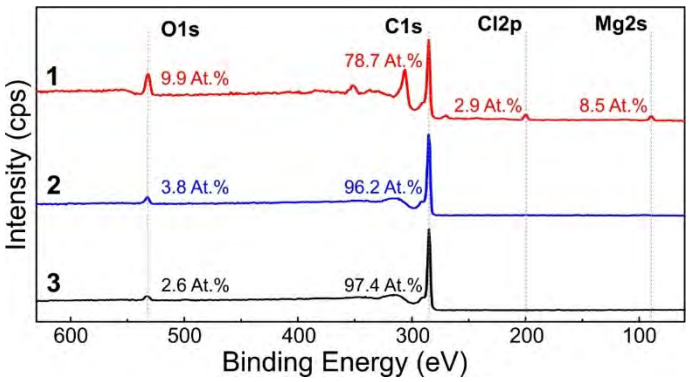

Fig. 4 - XPS survey spectra of (1) A-GLM, (2) P-GLM sample in contrast with (3) a graphite reference sample. High-resolution spectra are presented in Supporting Information.

The samples were examined by X-ray photon spectroscopy (XPS) in order to assess the role of the calcination process as well as the purity of the samples prepared. As presented in Fig. 4, the A-GLM displayed four major constituents including magnesium and chlorine. The high level of oxygen (~10 At. %) was also noted which is from the reduction by-product such as MgO, $Mg(OH)_2$ and $Mg(ClO_4)$ (See Supplementary Information for high resolution scans and their deconvolutions). The copious acid washing of the A-GLM improved the purity, but more than 6 atomic % magnesium was still observed, likely due to trapped Mg constituents located within various carbon matrices (e.g. MgO trapped in amorphous carbon) which could not be digested. Upon further processing including calcination and digestions (to form P-GLM), no traceable constituents were detected other than carbon and oxygen.

Thermogravimetric analysis of A-GLM (Fig. S2) resulted a 30% mass loss at the calcination temperature used here (570 °C) indicating oxidation of amorphous carbon. This was confirmed using infrared spectroscopy, where the A-GLM showing notable stretching and bending absorptions in the relevant regions, including C-C at 1610 cm^{-1} and C-H between 1180 and 960 cm^{-1} respectively[29]. These IR absorptions are absent in the P-GLM and the reference CVD-derived graphene (Fig. S3) materials.

A series of calcinations at lower temperatures (300 and 400 °C) was performed and the Raman spectra were obtained. The *D* and *2D* peaks from the A-GLM calcined at 300 and 500 °C are comparable to the *D* and *2D* peaks from the starting A-GLM material (Fig S4). Also, the lower calcination temperature correlates well with the observation of TGA shoulder peaks between 300 and 400 °C suggesting the presence of amorphous materials when A-GLM is calcinated at lower temperature. Temperatures between 550 and 600 °C are thus optimal for the oxidation and removal of amorphous carbon matrices.

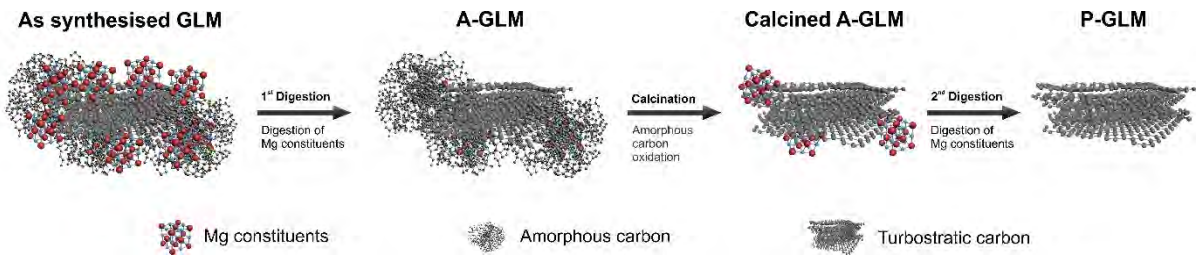

Scheme 2. Changes in the carbon and Mg constituents during digestions and calcination

As illustrated in Scheme 2, the first digestion removes the majority of Mg constituents whilst, the Mg exists in amorphous carbon cannot be digested. Upon the oxidation of the amorphous carbon *via* the calcination process, the Mg constituents are exposed. The remnants of the Mg can be digested using the same digestion protocol obtaining, affording pure turbostratic materials.

It has been reported that parallel polyaromatic molecular orientations appear around 400 °C when carbon materials are prepared by carbon monoxide disproportionation and the degree of the molecular orientation decreases when the material is subjected to oxidation[30]. Similar

to the previous report, the misalignment of the carbon layers can occur during the CO_2 reduction in the dry ice blocks or decomposition of the amorphous carbon in the calcination process. However, we rejected the possibility of the calcination process since the *d*-spacing from the XRD strongly suggested that the turbostratic carbons were formed prior to the calcination. On the other hand, progressive carbonisation of various carbon species may occur during the reductive decomposition of CO_2 and the concomitant oxidation of Mg. It has been reported previously that decomposition of carbon precursors produces turbostratic carbons at relatively lower temperatures than the temperature required for graphitisation[28,30,31]. Since the reduction of CO_2 and the oxidation of Mg is highly exothermic (~2000 °C), the temperature gradient within the reaction system (dry ice blocks, sublimation at -78 °C) cannot be ignored. Therefore, we hypothesise that the temperature within the reaction system may be ideal for the production of both amorphous and turbostratic carbons. Further studies are required to elucidate the precise mechanisms that lead to the formation of misaligned graphene layers.

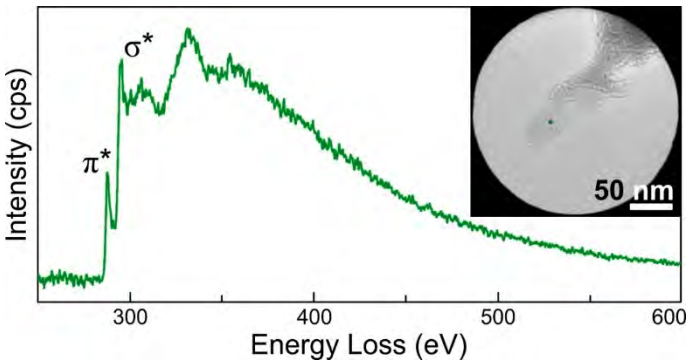

Fig. 5 - Electron energy loss spectrum of P-GLM (Inset: image of the measured area, no constituents other than carbon were noted).

The P-GLM was examined using an electron energy loss spectroscopy (EELS). The spectrum suggests (Fig. 5) that the material is graphitic in nature[32] but differs from pure graphene[33]. The peak at 330 eV is notably different from other graphite-like materials[32–34]. This peak is highly likely due to multiple scattering, originated from both thin and thick areas of the P-GLM.

4. Conclusion

In conclusion, calcination and digestion processes facilitated the isolation of turbostratic graphene-like materials, as illustrated in Scheme 2. Prior to the calcination, the A-GLM sample showed a broad *2D* Raman band similar to carbon containing few layers of graphene. A noticeable amount of impurities was also observed. However, no constituents other than carbon and oxygen were observed after the calcination and additional acid digestion. Furthermore, the *2D* Raman peak in the P-GLM shows a Raman *2D* band that is a single Lorentzian peak similar to that observed in a single-layer graphene. From the various experimental observations, it is clear that the calcination and subsequent and acid washing processes, when performed upon the A-GLM material, leads to the facile isolation of high-purity turbostratic P-GLMs. Based on the Raman spectroscopy results, the electronic structure for P-GLM can be approximated to single-layer graphenes. They possess a broadening of the *2D* feature due to the relaxation of the displacement representation Raman selection rules associated with the random orientation of the graphene layers with respect to each other. The unique electronic structure of turbostratic graphite coupled with the economic and scalable synthetic method described here may enable the development of applications such as molecular electronics and energy storage and conversion materials.

Acknowledgements

T.K, C.M and C.B acknowledge School of Environment and Natural Science and The Environmental Futures Research Institute for the financial support. The authors acknowledge Dr Barry Wood at the University of Queensland for his assistance in XPS analyses.

Appendix A. Supplementary data

Supplementary data associated with this article can be found, in the online version, at

References

[1] M. Xu, T. Liang, M. Shi, H. Chen, Graphene-like two-dimensional materials, Chem. Rev. 113 (2013) 3766–3798. doi:10.1021/cr300263a.

[2] K.S. Novoselov, V.I. Fal′ko, L. Colombo, P.R. Gellert, M.G. Schwab, K. Kim, A roadmap for graphene, Nature. 490 (2012) 192–200. doi:10.1038/nature11458.

[3] E.P. Randviir, D.A.C. Brownson, C.E. Banks, A decade of graphene research: Production, applications and outlook, Mater. Today. 17 (2014) 426–432. doi:10.1016/j.mattod.2014.06.001.

[4] R. Sengupta, M. Bhattacharya, S. Bandyopadhyay, A.K. Bhowmick, A review on the mechanical and electrical properties of graphite and modified graphite reinforced polymer composites, Prog. Polym. Sci. 36 (2011) 638–670. doi:10.1016/j.progpolymsci.2010.11.003.

[5] W.J. Lee, U.N. Maiti, J.M. Lee, J. Lim, T.H. Han, S.O. Kim, Nitrogen-doped carbon nanotubes and graphene composite structures for energy and catalytic applications, Chem. Commun. 50 (2014) 6818. doi:10.1039/c4cc00146j.

[6] A.K. Geim, Graphene: Status and Prospects, Sci. (80-.). 324 (2009) 1530–1534.

doi:10.1126/science.1158877.

[7] M. Yi, Z. Shen, A review on mechanical exfoliation for the scalable production of graphene, J. Mater. Chem. A. 3 (2015) 11700–11715. doi:10.1039/C5TA00252D.

[8] D.R. Dreyer, S. Park, C.W. Bielawski, R.S. Ruoff, Graphite oxide, Chem. Soc. Rev. 39 (2010) 228–240. doi:10.1039/b917103g.

[9] M.J. Allen, V.C. Tung, R.B. Kaner, Honeycomb carbon: A review of graphene, Chem. Rev. 110 (2010) 132–145. doi:10.1021/cr900070d.

[10] R.S. Edwards, K.S. Coleman, Graphene synthesis: relationship to applications, Nanoscale. 5 (2013) 38–51. doi:10.1039/C2NR32629A.

[11] A.C. Ferrari, D.M. Basko, Raman spectroscopy as a versatile tool for studying the properties of graphene, Nat. Nanotechnol. 8 (2013) 235–246. doi:10.1038/nnano.2013.46.

[12] J.A. Garlow, L.K. Barrett, L. Wu, K. Kisslinger, Y. Zhu, J.F. Pulecio, Large-Area Growth of Turbostratic Graphene on Ni(111) via Physical Vapor Deposition, Sci. Rep. 6 (2016) 19804. doi:10.1038/srep19804.

[13] S. Shallcross, S. Sharma, E. Kandelaki, O.A. Pankratov, Electronic structure of turbostratic graphene, Phys. Rev. B - Condens. Matter Mater. Phys. 81 (2010) 165105. doi:10.1103/PhysRevB.81.165105.

[14] U. Mogera, R. Dhanya, R. Pujar, C. Narayana, G.U. Kulkarni, Highly Decoupled Graphene Multilayers: Turbostraticity at its Best, J. Phys. Chem. Lett. 6 (2015) 4437–4443. doi:10.1021/acs.jpclett.5b02145.

[15] A.C. Ferrari, Raman spectroscopy of graphene and graphite: Disorder, electron-phonon coupling, doping and nonadiabatic effects, Solid State Commun. 143 (2007) 47–57. doi:10.1016/j.ssc.2007.03.052.

[16] L.G. Cançado, A. Reina, J. Kong, M.S. Dresselhaus, Geometrical approach for the study of G′ band in the Raman spectrum of monolayer graphene, bilayer graphene, and bulk graphite, Phys. Rev. B - Condens. Matter Mater. Phys. 77 (2008) 245408.

doi:10.1103/PhysRevB.77.245408.

[17] D.R. Lenski, M.S. Fuhrer, Raman and optical characterization of multilayer turbostratic graphene grown via chemical vapor deposition, J. Appl. Phys. 110 (2011). doi:10.1063/1.3605545.

[18] L.M. Malard, M.A. Pimenta, G. Dresselhaus, M.S. Dresselhaus, Raman spectroscopy in graphene, Phys. Rep. 473 (2009) 51–87. doi:10.1016/j.physrep.2009.02.003.

[19] N. Richter, Y.R. Hernandez, S. Schweitzer, J.S. Kim, A.K. Patra, J. Englert, I. Lieberwirth, A. Liscio, V. Palermo, X. Feng, A. Hirsch, K. Müllen, M. Kläui, Robust Two-Dimensional Electronic Properties in Three-Dimensional Microstructures of Rotationally Stacked Turbostratic Graphene, Phys. Rev. Appl. 7 (2017). doi:10.1103/PhysRevApplied.7.024022.

[20] Y. Cao, V. Fatemi, S. Fang, K. Watanabe, T. Taniguchi, E. Kaxiras, P. Jarillo-Herrero, Unconventional superconductivity in magic-angle graphene superlattices, Nature. 556 (2018) 43–50. doi:10.1038/nature26160.

[21] Y. Cao, V. Fatemi, A. Demir, S. Fang, S.L. Tomarken, J.Y. Luo, J.D. Sanchez-Yamagishi, K. Watanabe, T. Taniguchi, E. Kaxiras, R.C. Ashoori, P. Jarillo-Herrero, Correlated insulator behaviour at half-filling in magic-angle graphene superlattices, Nature. 556 (2018) 80–84. doi:10.1038/nature26154.

[22] A. Chakrabarti, J. Lu, J. Skrabutenas, T. Xu, Z. Xiao, J.A. Maguire, N.S. Hosmane, Conversion of carbon dioxide to few-layer graphene, J. Mater. Chem. 21 (2011) 9491. doi:10.1039/c1jm11227a.

[23] F. Negri, E. Di Donato, M. Tommasini, C. Castiglioni, G. Zerbi, K. M??llen, Resonance Raman contribution to the D band of carbon materials: Modeling defects with quantum chemistry, J. Chem. Phys. 120 (2004) 11889–11900. doi:10.1063/1.1710853.

[24] A. Milani, M. Tommasini, G. Zerbi, Carbynes phonons: A tight binding force field, J. Chem. Phys. 128 (2008) 064501. doi:10.1063/1.2831507.

[25] K. Kim, S. Coh, L.Z. Tan, W. Regan, J.M. Yuk, E. Chatterjee, M.F. Crommie, M.L. Cohen, S.G. Louie, A. Zettl, Raman spectroscopy study of rotated double-layer graphene: Misorientation-angle dependence of electronic structure, Phys. Rev. Lett. 108 (2012) 246103. doi:10.1103/PhysRevLett.108.246103.

[26] A.K. Kercher, D.C. Nagle, Microstructural evolution during charcoal carbonization by X-ray diffraction analysis, Carbon N. Y. 41 (2003) 15–27. doi:10.1016/S0008-6223(02)00261-0.

[27] Z.Q. Li, C.J. Lu, Z.P. Xia, Y. Zhou, Z. Luo, X-ray diffraction patterns of graphite and turbostratic carbon, Carbon N. Y. 45 (2007) 1686–1695. doi:10.1016/j.carbon.2007.03.038.

[28] S. Otani, A. Oya, J. Akagami, The effects of nickel on structural development in carbons, Carbon N. Y. 13 (1975) 353–356. doi:10.1016/0008-6223(75)90001-9.

[29] T.H. Kim, J.P. Sirdaarta, Q. Zhang, E. Eftekhari, J. St. John, D. Kennedy, I.E. Cock, Q. Li, Selective toxicity of hydroxyl-rich carbon nanodots for cancer research, Nano Res. (2017) 1–13. doi:10.1007/s12274-017-1838-2.

[30] M. Audier, A. Oberlin, M. Oberlin, M. Coulon, L. Bonnetain, Morphology and crystalline order in catalytic carbons, Carbon N. Y. 19 (1981) 217–224. doi:10.1016/0008-6223(81)90047-6.

[31] M. Inagaki, K. Fujita, Y. Takeuchi, K. Oshida, H. Iwata, H. Konno, Formation of graphite crystals at 1000-1200°C from mixtures of vinyl polymers with metal oxides, Carbon N. Y. 39 (2001) 921–929. doi:10.1016/S0008-6223(00)00210-4.

[32] F. Langenhorst, V.L. Solozhenko, ATEM-EELS study of new diamond-like phases in the B-C-N system, Phys. Chem. Chem. Phys. 4 (2002) 5183–5188. doi:10.1039/b206691b.

[33] Y. Liao, R. Pourzal, M.A. Wimmer, J.J. Jacobs, A. Fischer, L.D. Marks, Graphitic tribological layers in metal-on-metal hip replacements, Science (80-.). 334 (2011) 1687–1690. doi:10.1126/science.1213902.

[34] W. Zhou, S.J. Pennycook, J.-C. Idrobo, Probing the electronic structure and optical response of a graphene quantum disk supported on monolayer graphene, J. Phys. Condens. Matter. 24 (2012) 314213. doi:10.1088/0953-8984/24/31/314213.